Regular Article

PHYSICAL CHEMISTRY RESEARCH
Published by the
Iranian Chemical Society
www.physchemres.org
info@physchemres.org

Phys. Chem. Res., Vol. 12, No. 3, 753-762, September 2024
DOI: 10.22036/pcr.2024.413249.2403

Molecular Docking and Molecular Dynamics Simulations of Bendamustine Functionalized Al/B-N/P Nanocages as Potential Inhibitors of Cellular Tumor Antigen

Nosrat Madadi Mahani[a,*], Roya Yosefelahi[a] and Reza Behjatmanesh-Ardekani[b]

[a]*Department of Chemistry, Payame Noor University, 19395-4697, Tehran, Iran*

[b]*Department of Chemical Engineering, Faculty of Engineering, Ardakan University, P. O. Box: 184, Ardakan, Iran*

(Received 25 August 2023, Accepted 13 February 2024)

Drug delivery based on nanocages is helpful in nanomedicine with the minimum side effects and targeting drugs in the cancer cell. Bendamustine, an anti-cancer drug, inhibits the activity of cancer cells in humans and is broadly used in the therapy of breast cancer. The interaction of single Bendamustine and Bendamustine@Al/B-N/P nanocages with P53 protein was studied. In this study, molecular docking and molecular dynamics simulations (MD) were conducted to investigate the interaction of some of the Bendamustine, Al/B-N/P nanocages with the P53 protein. The best pose of the configuration of Bendamustine and Bendamustine@Al/B-N/P nanocages in the active sites of the P53 protein results in negative binding energies. Complexes of Bendamustine@$B_{12}N_{12}$ and Bendamustine@$B_{12}P_{12}$ with P53 protein have the most binding energy. In addition, MD simulation was done on the stable complexes with high binding energy to recognize the structural changes in the complexes of Bendamustine, Bendamustine@$B_{12}N_{12}$, and bendamustine@$B_{12}P_{12}$ nanocages with P53 protein. Studies illustrated that $B_{12}N_{12}$ and $B_{12}P_{12}$ could serve as drug carriers for delivering the Bendamustine drug in a targeted procedure for inhibiting the P53 protein. In-silico studies are important parts of the structure-based drug design process that displayed that nanocages are suitable sensors for the Bendamustine drug.

Keywords: Binding energy, Drug carriers, Root mean square displacement, Radius of gyration, Anti-cancer drug

INTRODUCTION

Bendamustine, 4-(5-(Bis (2-chloroethyl) amino)-1-methyl-1H-benzo [d]imidazol-2-yl") butyric acid, consists of a butyric acid side chain, a benzimidazole ring, and a 2-chloroethylamine alkylating group [1]. It is an alkylating and antimetabolite agent [2] used as a chemotherapeutic drug [3]. Also, the bendamustine drug has been used in the treatment of diseases such as chronic lymphocytic leukemia (CLL), indolent lymphoma, and refractory rituximab illness [4]. Prosperous and acceptable delivery of Bendamustine as an anticancer drug is essential in the treatment of non-Hodgkin lymphoma (NHL), multiple myeloma, and chronic lymphatic leukemia (CLL) patients. A perfect drug delivery should have suitable physicochemical and biocompatibility properties. Nanocages (fullerene-like nanomaterials) are widely used in pharmaceutical applications due to their chemical and physical properties in specific band gaps [5-7]. Nanocages, as nanocarriers, can make drug delivery to cells easier and can decrease the toxic effects of anti-cancer drugs [8]. Recently, it has been reported that boron nitride ($B_{12}N_{12}$) and boron phosphide ($B_{12}P_{12}$) nanocages can be used for drug delivery due to their nontoxic nature and great adsorbing capacity [9]. The effect of chemical order on the physicochemical and structural properties of $B_{12}N_{12}$ nanocages has been investigated by Escobedo-Morales *et al.* [10] with molecular dynamics and density functional theory approaches.

Molecular docking analysis has an important role in computer-aided drug design (CADD) and the biology of

*Corresponding author. E-mail: nmmadady@gmail.com

structural molecular biology [11]. Also, this computational method is used for evaluating the binding affinity between protein and ligand [12]. The use of molecular dynamics simulation can be useful in designing drug delivery systems on an atomic scale and obtaining drug stability. Ramana *et al.* have performed investigations of quantum mechanical and molecular docking on the anti-cancer drug Bendamustine. They have applied the DNA binding protein of cellular tumor antigen P53 for molecular docking [13]. Shyma Mary *et al.* have investigated the interaction of the Sorbic acid drug with fullerene-like nanocages by molecular docking and the DFT method [14].

Studies of complexes of $B_{12}N_{12}$ and $B_{12}CaN_{12}$ nanocages with the Penicillamine drug as potential inhibitors of proinflammatory cytokines have been performed using ADMET, molecular docking, and DFT analysis [15]. Also, single-walled carbon nanotubes as drug delivery systems for the anticancer Doxorubicin have been studied by molecular dynamics (MD) simulations [16]. Apoferritin-nanocage has been used as drug delivery for the combination of doxorubicin and docetaxel drugs using molecular docking [17]. $B_{12}N_{12}$ has been investigated as a drug carrier for the 5-fluorouracil (5FU) drug with the DFT approach by Aktaş and coworkers [18]. Also, they have found that both the 5FU and 5FU@$B_{12}N_{12}$ complexes are helpful in inhibiting vascular endothelial growth factor receptors with the use of docking scores and interaction energies from docking calculations. Studies of molecular docking simulations have been performed on the encapsulation of antiviral favipiravir drug into carbon nanotubes (C-C, Al-N) with dispersion-corrected DFT calculation [19]. Also, the inflammatory activity of thiazole by $B_{12}N_{12}$ and OH-$B_{12}N_{12}$ nanoclusters has been studied with molecular docking, ADMET, and DFT calculations [20]. Adsorption behavior of glycine with $B_{16}N_{16}$ and $B_{12}N_{12}$ nanoclusters has been investigated as potential inhibitors of proinflammatory cytokines by molecular modeling and simulation [21].

Recently, the interaction of bendamustine anti-cancer drug with Al/B-N/P nanocages has been studied by the DFT approach and the B3LYP/6-31G(d,p) calculations and has demonstrated that $B_{12}P_{12}$ and $B_{12}N_{12}$ nanocages are suitable for drug delivery. All studied nanocages were suitable nanocarriers for detecting the Bendamustine drug. Based on their desorption time, $B_{12}P_{12}$ and $B_{12}N_{12}$ nanocages demonstrated more favorable for drug delivery than $Al_{12}P_{12}$ and $Al_{12}N_{12}$ [22].

COMPUTATIONAL DETAILS

The structures of the Bendamustine drug and complexes of Bendamustine with Al/B-N/P nanocages as ligands are obtained from the output from DFT optimization at B3LYP/6-31G(d,p) level theory, in which the most stable configurations were selected. The structures of complexes of Bendomustine with $B_{12}P_{12}$, $B_{12}N_{12}$, $Al_{12}N_{12}$, and $Al_{12}P_{12}$ nanocages are shown in Fig. 1.

Molecular Docking Methods

Molecular docking, a suitable method for evaluating the binding affinity between protein and ligand, was performed using the Auto Dock 1.5.6 software package [23]. The crystal structure of the DNA binding protein of Cellular Tumor Antigen P53 (PDB ID: 6SHZ) was acquired from the Protein Data Bank (PDB) [24]. In the first step, the protein model was improved by increasing hydrogen atoms using the Auto Dock builder module. The protein molecule was retained rigid, while all the torsion angles in the small molecules except the nanocage atoms were set to rotate freely. The grid box size and center were set at 70 × 70 × 70 $Å^3$ and 119.547, 89.021, and -26.722 for x-, y-, and z-coordinates to allow the ligand to rotate freely.

To get the optimized scoring function and the most conformation with 200 separated docking calculations, including the full 25,000,000 energy assessments, the Lamarckian genetic algorithm [25] was employed. Also, a mutation rate of 0.02, the maximum number of 27,000 generations, a crossover rate of 0.80 with cluster tolerance of 2 Å, and a population size of 150 were used. Gasteiger charges [26] are calculated for allocating atomic charges. The optimal docking pose was selected based on the lowest free energy of binding in the highest-populated cluster and interactions of the ligand with active sites of protein were analyzed automatically using the PyMOL molecular graphics system of docking as a powerful molecular viewer with exceptional 3D capabilities [27].

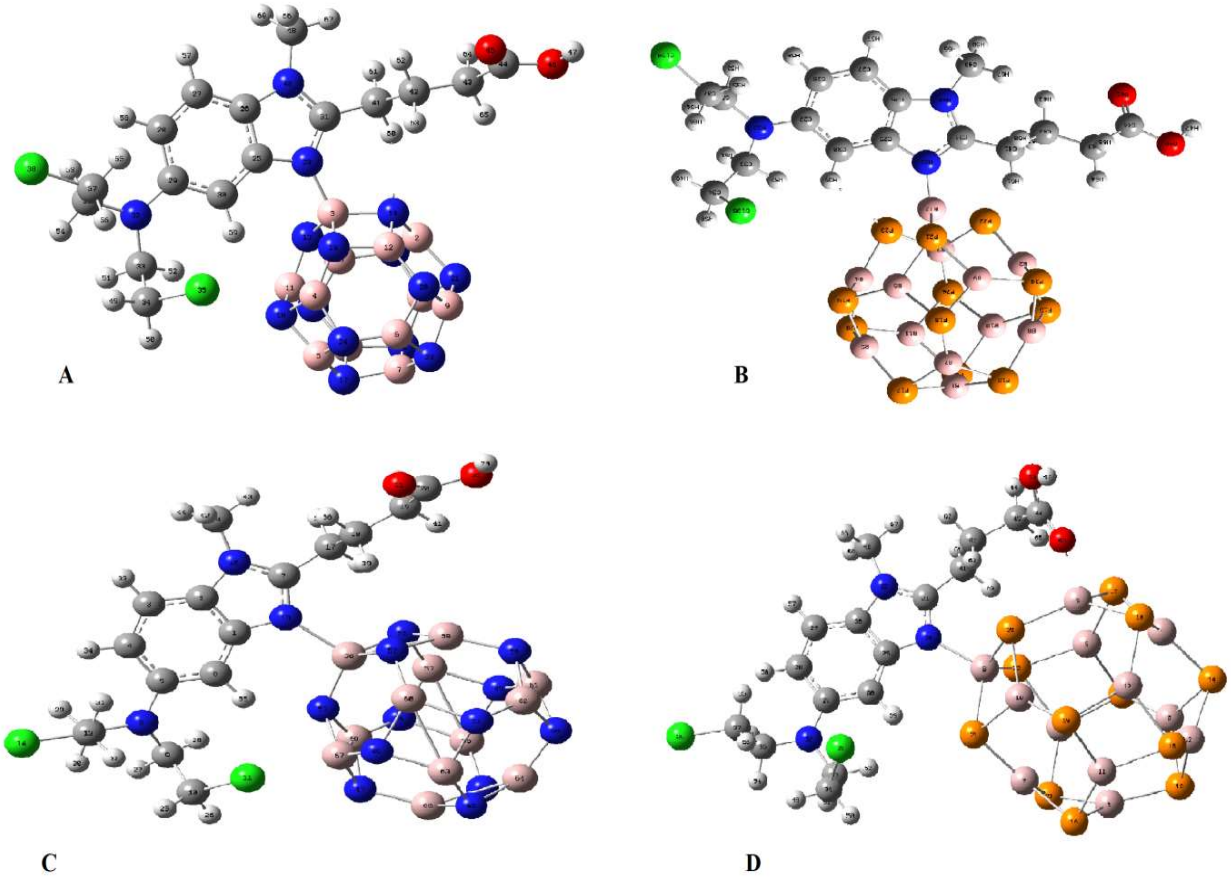

Fig. 1. The optimized structures of Bendamustine@$B_{12}N_{12}$ (A), Bendamustine@$B_{12}P_{12}$ (B), Bendamustine@$Al_{12}N_{12}$ (C) and Bendamustine@$Al_{12}P_{12}$ (D).

Molecular Dynamics Simulations

Molecular dynamics (MD) simulations were carried out in order to investigate protein folding, protein stability, conformational changes, dynamical behavior, and molecular recognition. The properties of the dynamic and the flexibility of the protein of cellular tumor antigen p53 were studied according to the topology of local contacts by the MD simulations. The Gromacs 2019.6 package with the Amber99SB force field [28] was used for the simulation of cellular tumor antigen P53 protein in free form and its complex with one ligand (Bendamustine, Bendamustine@$B_{12}N_{12}$ nanocages, and Bendamustine@$B_{12}P_{12}$ nanocages) in a cubic box of water. The most stable and best poses of conformation with the lowest docking free energy were selected for MD simulations. The ACPYPE tool based on Python was used for the parameters of the force field [29]. The tip3p model was applied for implicating water molecules, and suitable counter ions were applied for the neutrality of charge in the systems. The steepest descent method was applied to each system for energy minimization. In the following, the procedure of position restraint was done with NPT (constant temperature and constant pressure) and NVT (constant temperature and constant volume) ensembles. The constant temperature of 310 K and the constant pressure of 1.0 bar were utilized at a time duration of 200 ps for systems equilibration [30-33]. The Particle-Mesh Ewald method for the computation of interactions of van der Waals and the Lincs (Linear Constraint Solver) algorithm for constraints of the covalent bonds were used [34-35]. In the end, trajectories with a length of 150 ns and a time integration step of 2 fs were recorded using the leap-frog algorithm.

Table 1. Molecular Docking Properties for the Best-docked Structure (Energies are in kcal mol^{-1})

System	ΔG binding	ki (μM)	Intermolecular energy	Internal energy
Protein-Bendamustine	-6.34	22.70	-9.02	-0.87
Protein-Bendamustine@$B_{12}N_{12}$	-5.77	57.90	-10.47	-2.37
Protein-Bendamustine@$B_{12}P_{12}$	-5.82	54.09	-12.13	-1.54
Protein-Bendamustine@$Al_{12}N_{12}$	-5.72	64.56	-12.58	-2.18
Protein-Bendamustine@$Al_{12}P_{12}$	-5.67	68.41	-11.53	-1.84

RESULTS AND DISCUSSION

Molecular Docking Study

The molecular docking calculations were performed for systems of P53 protein and bendamustine drug and complexes of bendamustine with $B_{12}P_{12}$, $B_{12}N_{12}$, $Al_{12}N_{12}$, and $Al_{12}P_{12}$ nanocages as ligands. Docking properties for the best configuration of P53 protein-ligand, such as binding energy, intermolecular energy, inhibition constant (kI), and internal energy for the best-docked structures, have been listed in Table 1. The binding energy with negative values illustrated that the binding nature of these compounds as the drug with the P53 protein is strong, and the simple drug has the highest binding energy. Also, the simple drug has the smallest inhibition constant (kI). Almost all systems have an inhibition constant close to that of the pure drug.

Structures of the best configurations of protein-ligand have been generated by using the PyMOL program, as illustrated in Figs. 2 and 3. Also, the hydrophobic contacts for binding to the ligand are shown in Figs. 2 and 3. Simple drugs form hydrogen bonds with Asn200, His233, and Glu198. Bendamustine@$B_{12}N_{12}$ and Bendamustine@$Al_{12}P_{12}$ form one hydrogen bond with Lys139 and His233, respectively. However, both Bendamustine@$B_{12}P_{12}$ and Bendamustine@$Al_{12}N_{12}$ form two hydrogen bonds with Gln100 and Thr102. The number of hydrogen bonds in four systems compared to simple Bendamustine is less, but the length of hydrogen bonds is suitable. All studied compounds get grooved within the binding pocket on the P53 protein basis on the electrostatic surfaces.

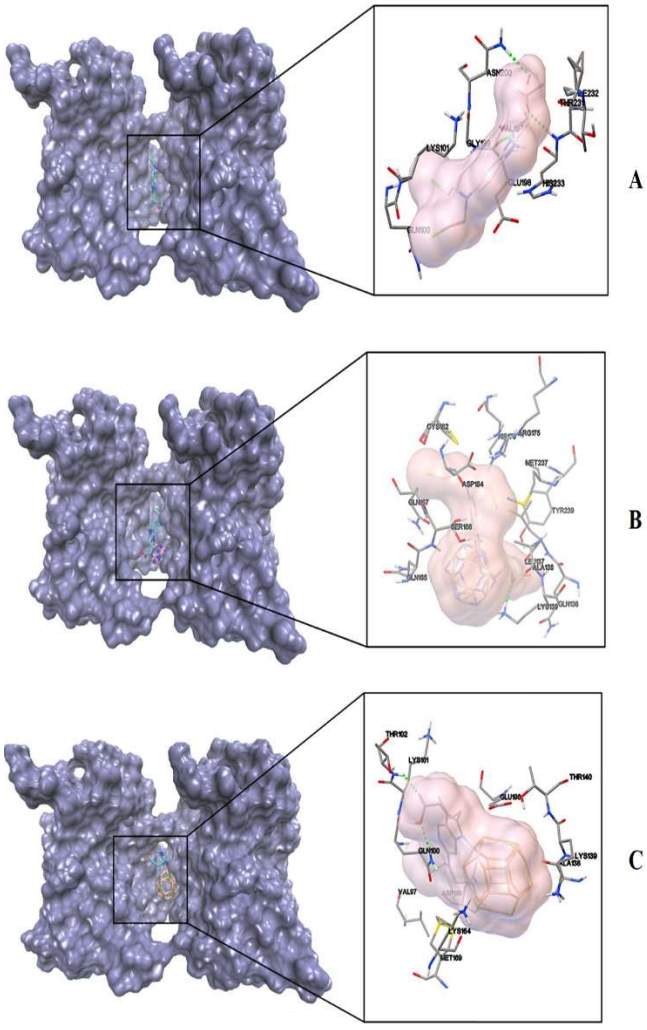

Fig. 2. The docked protein-ligand complexes with hydrogen bond interactions: Bendamustine (A), Bendamustine@$B_{12}N_{12}$ (B), and Bendamustine@$B_{12}P_{12}$ (C).

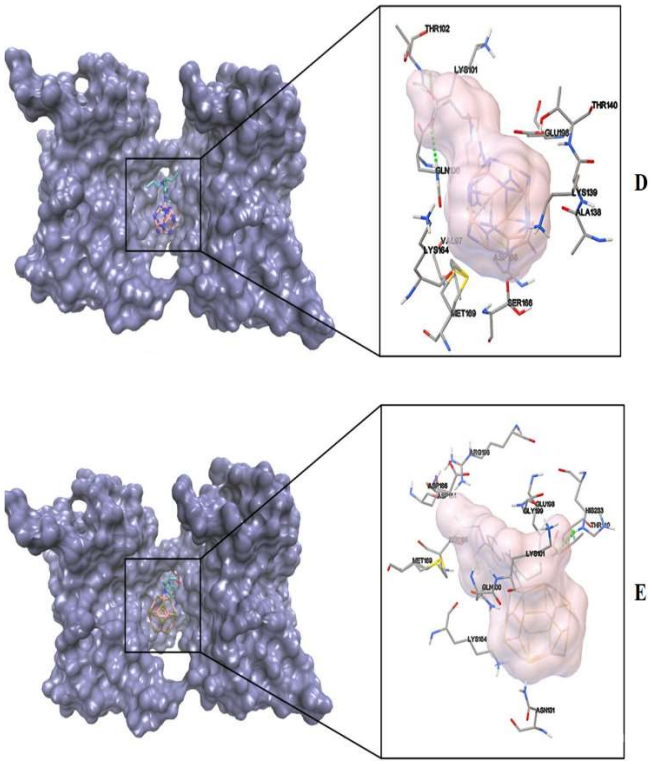

Fig. 3. The docked protein-ligand complexes with hydrogen bond interactions: Bendamustine@$Al_{12}N_{12}$ (D) and Bendamustine@$Al_{12}P_{12}$ (E).

Molecular Dynamics Simulations

Based on the results of DFT calculation [19] and molecular docking, molecular dynamics simulation was carried out to explore the stability of the Bendamustine, Bendamustine@$B_{12}N_{12}$, and Bendamustine@$Bl_{12}P_{12}$ as ligands to the binding sites of the P53 protein. According to the topology of local contacts, the dynamic properties and flexibility of the P53 protein were studied by computational methods. The time of simulation of 150 ns in creating the ligand complexes was subjected.

The Root mean square displacement (RMSD) of complexes was studied to investigate their dynamic properties and the structure of the complexes. The RMSD was defined based on Eq. (1):

$$RMSD = \sqrt{\frac{\sum_{i=0}^{n} \delta_i^2}{N}} \quad (1)$$

Where δ displays the interval between the n pairs of analogous atoms and n displays the total number of atoms evaluated in the computation. The backbone RMSD of the P53 protein is displayed in Fig. 4.

The RMSD of protein- Bendamustine has more fluctuation than protein-Bendamustine@$B_{12}N_{12}$ and protein-Bendamustine@$B_{12}P_{12}$. The RMSD of protein-Bendamustine@$B_{12}N_{12}$ and protein-Bendamustine@$B_{12}P_{12}$ were more stable during stabilization in comparison to protein-Bendamustine. The RMSD of protein-Bendamustine received a maximum deviation of 15 ns.

Also, overall, with a simulation period of 150 ns, the hydrogen bond interactions are illustrated in Fig. 5. More hydrogen bonds between Bendamustine@$B_{12}N_{12}$ and water molecules than Bendamustine@$B_{12}P_{12}$, prepare an appropriate environment for the drug molecule in the system of Bendamustine@$B_{12}N_{12}$ within the transmission to the cell. The plots of root mean square fluctuations (RMSFs) were used for evaluating the motility and flexibility of the residues (Fig. 6). RMSF was indicated as Eq. (2):

$$RMSF(i) = \sqrt{(R_i - (R_i)^2)} \quad (2)$$

where R_i represents the position vector of "i" atom. The greater flexibility of a complex is related to the higher values of RMSF.

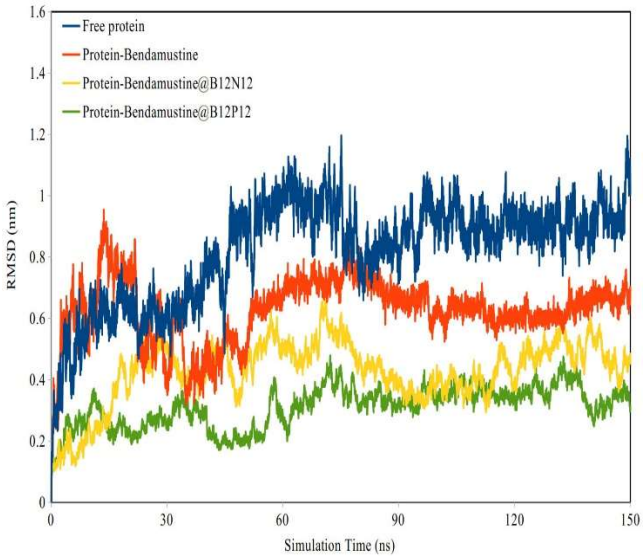

Fig. 4. The RMSD of the backbone atom of the P53 protein over a time period of 150 ns.

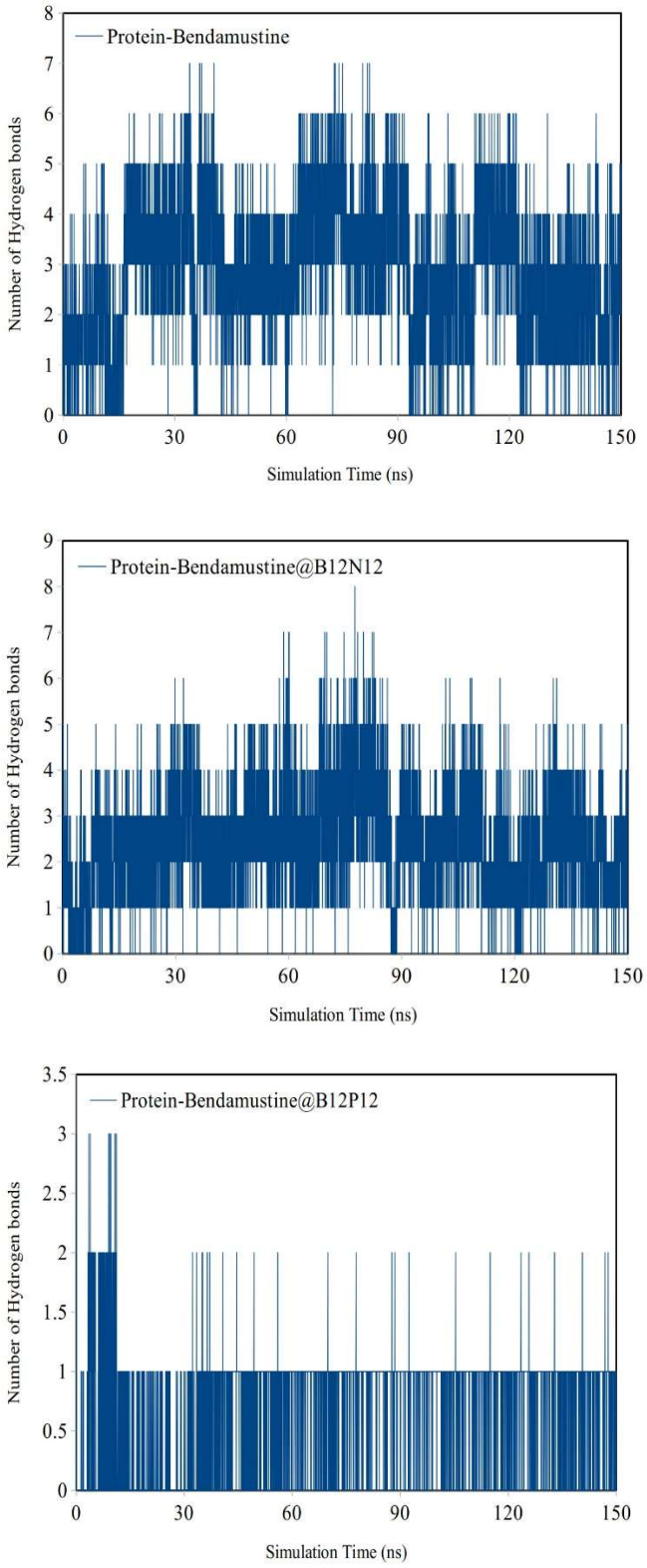

Fig. 5. The total number of hydrogen bonds produced during the simulation period of 200 ns.

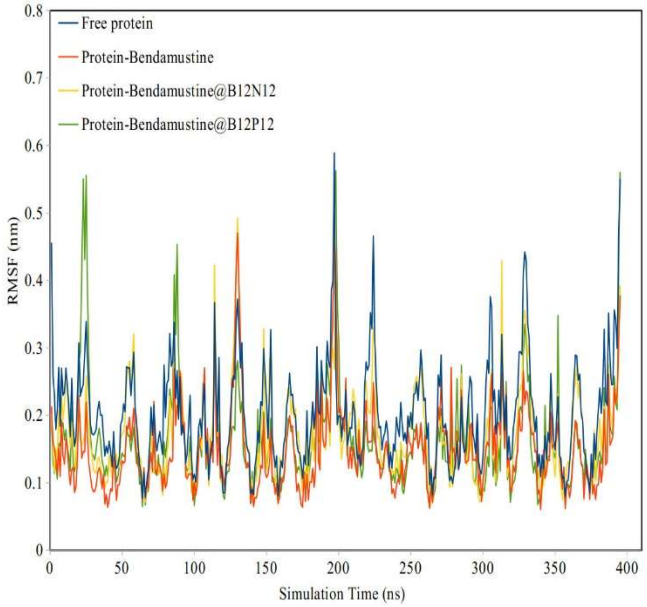

Fig. 6. RMSF values of backbone atoms of P53 protein during the entire simulation time, in the absence and presence of Bendamustine, Bendamustine@$B_{12}N_{12}$, and Bendamustine@$B_{12}P_{12}$.

The RMSFs of all complexes illustrated the fluctuation under 0.6 nm. The complex Bendamustine@$B_{12}P_{12}$ with the P53 protein displayed more deviation in the time simulation. The RMSFs of the complexes Bendamustine and Bendamustine@$B_{12}N_{12}$ with the P53 protein demonstrated almost the same deviation (Fig. 6). The most stable residues of the caspase-3 protein are those whose RMSF value is less than 0.20 nm.

The radius of gyration (R_g) was used for the analysis of the structural flexibility of the complexes, which is defined as the root mean square distance of the objects from each atom of protein to their center of mass and is a criterion for the compactness of protein. The higher values of R_g signify that the protein's compactness is looser and weaker. The R_g was defined based on Eq. (3):

$$R_g = \sqrt{\frac{\sum_{i=1}^{N}(r_i - r_{conf})^2}{N}} \quad (3)$$

where N denotes the total number of protein atoms, r_i signifies an atom's position, and r_{conf} represents the protein's center of mass.

The graphs of R_g the P53 protein with three ligands are represented in Fig. 7. These complexes are steady within the simulation of 150 ns. The plots of R_g have the same patterns as the average R_g values in the region at 2.4 nm. Furthermore, at simulation times 50-70 ns, the free P53 protein deviates from 2.4 nm. R_g values of Protein-Bendamustine@$B_{12}N_{12}$ and Bendamustine@$B_{12}P_{12}$ are almost the same.

With investigation values of solvent-accessible surface area (SASA), the stability and susceptibility of proteins to solvent molecules can be evaluated (Fig. 8). The lower SASA value of the protein in the complex displays its relatively compact nature compared to the pure structure. The maximum values of SASA related to protein-Bendamustine@$B_{12}P_{12}$ and protein-Bendamustine have the least amount of SASA. On the other hand, the SASA values of protein-Bendamustine@$B_{12}P_{12}$ are closer to protein-Bendamustine.

Molecular dynamics (MD) simulation is a method in the design of drug delivery mechanisms that is used as an in silico means in computationally assisted design (CAD). MD simulations can anticipate the intermolecular interactions and properties of drugs at the atomistic level and evaluate and control the conformational behaviors of the atoms and

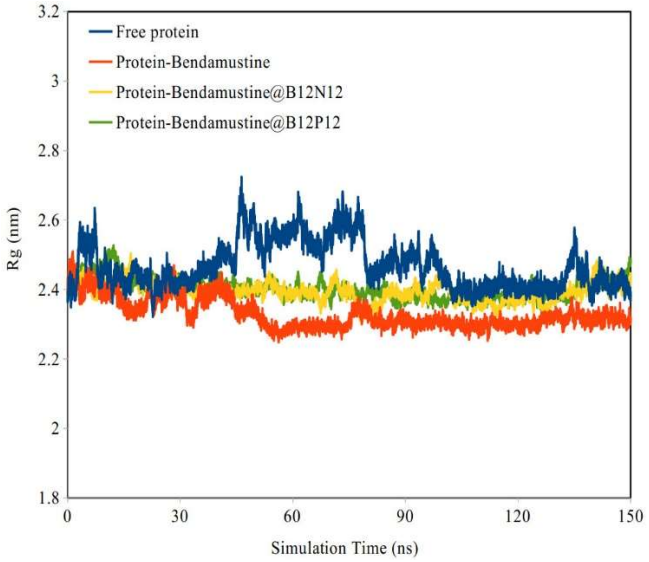

Fig. 7. Time dependence of the radius of gyration (R_g) for the backbone atoms of P53 protein during the simulation, in the absence and presence of Bendamustine, Bendamustine@$B_{12}N_{12}$, and Bendamustine@$B_{12}P_{12}$.

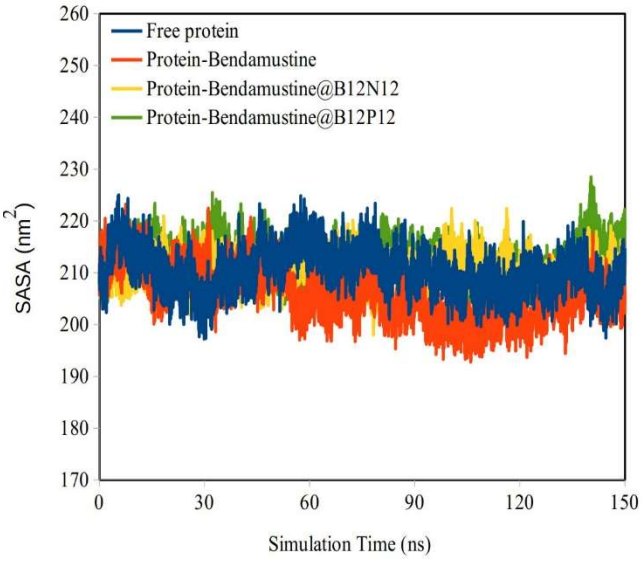

Fig. 8. Total SASA of P53 protein during the simulation, in the absence and presence of Bendamustine, Bendamustine@$B_{12}N_{12}$, and Bendamustine@$B_{12}P_{12}$.

molecules, which accredit the results of the molecular docking. We suggest that the adsorption of Bendamustine drug on the doped nanocages be investigated which causes an increasing solubility of the drug and has greater more thermodynamic advantages than pure nanocages.

CONCLUSION

The molecular docking is performed to explore detailed information about systems of the Bendamustine, Bendamustine@$B_{12}N_{12}$, Bendamustine@$B_{12}P_{12}$, Bendamustine@$Al_{12}N_{12}$, and Bendamustine@$Al_{12}P_{12}$-P53 proteins. The active sites of the P53 protein in interaction with the studied ligands are specified. In addition, the molecular dynamics simulation of Bendamustine, Bendamustine@$B_{12}N_{12}$, and Bendamustine@$B_{12}P_{12}$ were applied to accurately infer the conformational changes in ligand-protein complexes. The analysis of the MD results reveals that the studied ligands move into the active site due to the formation of hydrogen bonds and polar interactions. The best stable complex has the highest mean RMSD, which resulted from analysis of the MD trajectories. The complexes of Bendamustine and Bendamustine@$B_{12}N_{12}$ with P53 protein are stable. The results clearly illustrated that $B_{12}N_{12}$

and $B_{12}P_{12}$ could serve as drug carriers for delivering Bendamustine drug in a targeted procedure. The $B_{12}N_{12}$ and $B_{12}P_{12}$-based drug delivery vehicles can be suitable anticancer therapeutic formulations and are helpful in inhibiting the P53 protein. Also, these complexes can be used in the identification and development of novel compounds.

ACKNOWLEDGMENTS

We gratefully thank Payam Noor University for its financial support. The authors would like to express their appreciation to the Department of Chemistry at this university for providing research facilities.

REFERENCES

[1] Leoni, L. M., Bendamustine: rescue of an effective antineoplastic agent from the mid-twentieth century. *Semin. Hematol.* **2011**, *1*, S4-S11, DOI: 10.1053/j.seminhematol.2011.03.002.

[2] Nowak, D.; Boehrer, S.; Brieger, A.; Kim, S. Z.; Schaaf, S.; Hoelzer, D.; Mitrou, P. S.; Weidmann, E.; Chow, K. U., Upon drug-induced apoptosis in lymphoma cells X-linked inhibitor of apoptosis (XIAP) translocates from the cytosol to the nucleus. *Leuk Lymphoma* **2004**, *45*, 1429-1436, DOI: 10.1080/1042819042000198858.

[3] Friedberg, J. W.; Cohen, P.; Chen, L.; Robinson, K. S.; Forero-Torres, A.; La Casce, A. S.; Fayad, L. E.; Bessudo, A.; Camacho, E. S.; Williams, M. E.; H van der Jagt, R.; W Oliver, J.; Cheson, B. D., Bendamustine in patients with rituximab-refractory indolent and transformed non-Hodgkin's lymphoma: results from a phase II multicenter, single-agent study. *J. Clin. Oncol.* **2008**, *26*, 204, DOI: 10.1200/JCO.2007.12.5070.

[4] Kath, R.; Blumenstengel, K.; Fricke, H. J.; Hoffken, K., Bendamustine monotherapy in advanced and refractory chronic lymphocytic leukemia. *J. Cancer Res. Clin. Oncol.* ***20*01**, *127*, 48-54, DOI: 10.1007/s004320000180.

[5] Pan, M.; Yang, J.; Liu, K.; Yin, Z.; Ma, T.; Liu, S.; Xu. L.; Wang, S., Noble metal nanostructures materials for chemical and biosensing systems. *Nanomaterials* **2020**, *10*, 209-234, DOI: 10.3390/nano10020209.

[6] Naderi, H. R.; Sobhani-Nasab, A.; Rahimi-Nasrabadi, M.; Ganjali, M. R., Decoration of nitrogen doped reduced graphene oxide with cobalt tungstate nano particles for use in high performance supercapacitors. *Appl. Surf. Sci.* **2017**, *423*, 1025-1034, DOI: 10.1016/j.apsusc.2017.06.239.

[7] Sherafati, M.; Rad, A. S.; Ardjmand, M.; Heydarinasab, A.; Peyravi, M.; Mirzaei, M., Beryllium oxide (BeO) nano tube provides excellent surface towards adenine adsorption: A dispersion corrected DFT study in gas and water phases. *Curr. Appl. Phys.* **2018**, *18*, 1059-1065, DOI: 10.1016/j.cap.2018.05.024.

[8] Park, K., Facing the Truth about Nanotechnology in Drug Delivery. *ACS Nano* **2013**, *7*, 7442-7447, DOI: 10.1021/nn404501g.

[9] Wang, Q.; Sun, Q.; Jena, P.; Kawazoe, Y., Potential of AlN Nanostructures as Hydrogen Storage Materials. *ACS Nano* **2009**, *3*, 621-626, DOI: 10.1021/nn800815e.

[10] Escobedo-Morales, A.; Tepech-Carrillo, L.; Bautista-Hernandez, A.; Camacho-Garcia, J. H.; Cortes-Arriagada, D.; ChigoAnota, E., Effect of chemical order in the structural stability and physicochemical properties of $B_{12}N_{12}$ fullerenes. *Sci. Rep.* **2019**, *9*, 16521-16532, DOI: 10.1038/s41598-019-52981-1.

[11] Ramesh, P.; Lydia Caroline, M.; Muthu, S.; Narayana, B.; Raja, M.; Aayisha, S., Spectroscopic and DFT studies, structural determination, chemical properties and molecular docking of 1-(3-bromo-2-thienyl)-3-[4-(dimethylamino)-phenyl]prop-2-en-1-one. *J. Mol. Struct.* **2020**, *1200*, 127123, DOI: 10.1016/J.MOLSTRUC.2019.127123.

[12] Rahuman, M. H.; Muthu, S.; Raajaraman, B. R.; Raja, M.; Umamahesvari, H., Investigations on 2-(4-Cyanophenylamino) acetic acid by FT-IR, FT-Raman, NMR and UV-Vis spectroscopy, DFT (NBO, HOMO-LUMO, MEP and Fukui function) and molecular docking studies. *Heliyon* **2020**, *6*, e04976-e04987, DOI: 10.1016/j.heliyon. 2020. E04976.

[13] Venkata Ramana, P.; Sundius, T.; Muthu, S.; Chandra Mouli, K.; Rama Krishna, Y.; Venkata Prasad, K.; Niranjana Devi, R.; Irfan, A.; Santhamma, C., Spectroscopic, quantum mechanical, electronic excitation properties (Ethanol solvent), DFT

investigations and molecular docking analysis of an anti-cancer drug Bendamustine. *J. Mol. Struct.* **2022**, 1253, 132211-132235, DOI: 10.1016/j.molstruc.2021.132211.

[14] Shyma Mary, Y.; Sheena Mary, Y.; Ullah, Z., Computational Study of Sorbic Acid Drug Adsorption onto Coronene/ Fullerene/Fullerene-Like $X_{12}Y_{12}$ (X = Al, B and Y = N, P) Nanocages: DFT and Molecular Docking Investigations. *J. Clust. Sci.* **2022**, *33*, 1809-1819, DOI: 10.1007/s10876-021-02106-4.

[15] Cao, Y.; Khan, A.; Balakheyli, H.; KayLup, A. N.; Ramezani Taghartapeh, M.; Mirzaei, H.; Khandoozi, S. R.; Soltani, A.; Aghaei, M.; Heidari, F.; Sarkar, S. M.; Albadarin, A. B., Penicillamine functionalized $B_{12}N_{12}$ and $B_{12}CaN_{12}$ nanocages act as potential inhibitors of proinflammatory cytokines: A combined DFT analysis, ADMET and molecular docking study. *Arab. J. Chem.* **2021**, *14*, 103200-103216, DOI: 10.1016/j.arabjc.2021.103200.

[16] Pakdel, M.; Raissi, H.; Shahabi, M., Predicting doxorubicin drug delivery by single-walled carbon nanotube through cell membrane in the absence and presence of nicotine molecules: a molecular dynamics simulation study. *J. Biomol. Struct. Dyn.* **2020**, *38*, 1488-1498, DOI: 10.1080/07391102.2019.1611474.

[17] Ghosh, S.; Mohapatra, S.; Thomas, A.; Bhunia, D.; Saha, A.; Das, G.; Jana, B.; Ghosh, S., Apoferritin-nanocage delivers combination of microtubule and nucleus targeting anticancer drugs. *ACS Appl. Mater. Interfaces* **2016**, *8*, 30824-30832, DOI: 10.1021/acsami.6b11798.

[18] Aktas, A.; Nassif, W.; Sayin, K., Investigations of structural, spectral (IR, 1 H-, 9 F-, 11B-, 13C-, 15 N-, 17O-NMR) and anticancer properties of 5FU@$B_{12}N_{12}$ complexes. *Chem. Pap.* **2021**, *75*, 1727-1737, DOI: 10.1007/s11696-020-01433-6.

[19] Albarakati, R.; Al-Qurashi, O.; Safi, Z.; Wazzan, N., A dispersion-corrected DFT calculation on encapsulation of favipiravir drug used as antiviral against COVID-19 into carbon-, boron-, and aluminum-nitride nanotubes for optimal drug delivery systems combined with molecular docking simulations. *Struct. Chem*. **2023**, DOI: 10.1007/s11224-023-02182-4.

[20] Pan, F.; Turki Jalil, A.; Alsaikhan, F.; Adil, M.; Kadhim, A. J.; Al-azem Amran, D. A.; Abosaooda, M.; Altamimi, A. S.; Dhiaa Younis, S. M.; Ng Kay Lup, A.; Tavassoli, S.; Balakheyli, H.; Soltani, A., DFT, molecular docking, and ADMET studies for the adsorption behavior and anti-inflammatory activity of thiazole by $B_{12}N_{12}$ and OH-$B_{12}N_{12}$ nanoclusters. *Diam. Relat. Mater.* **2023**, *136*, 110044-110054, DOI: 10.1016/j.diamond.2023.110044.

[21] Gao, S.; Khan, A.; Nazari, M.; Mirzaei, H.; Ng Kay Lup, A.; Baei, M. T.; Chandiramouli, R.; Soltani, A.; Salehi, A.; Javan, M.; Jokar, M. J.; Pishnamazi, M.; Nouri, A., Molecular Modeling and Simulation of glycine functionalized $B_{12}N_{12}$ and $B_{16}N_{16}$ nanoclusters as potential inhibitors of proinflammatory cytokines. *J. Mol. Liq.* **2021**, *343*, 117494-117809, DOI : 10.1016/j.molliq.2021.117494.

[22] Madadi Mahani, N.; Behjatmanesh-Ardekani, R.; Yosefelahi, R., Adsorption of bendamustine anti-cancer drug on Al/B–N/P nanocages: A comparative DFT study. *J. Serb. Chem. Soc.* **2022**, *87*, 1157-1170, DOI: 10.2298/JSC220312046M.

[23] Morris, G. M.; Huey, R.; Lindstrom, W.; Sanner, M. F.; Belew, R. K.; Goodsell, D. S.; Olson, A.J., AutoDock4 and AutoDockTools4: Automated docking with selective receptor flexibility. *J. Comput. Chem.* **2009**, *30,* 2785-2791, DOI: 10.1002/jcc.21256.

[24] Bauer, M. R.; Kramer, A.; Settanni, G.; Jones, R. N.; Ni, X.; Khan Tareque, R.; Fersht, A. R.; Spencer, J.; Joerger, A. C., Targeting Cavity-Creating p53 Cancer Mutations with Small-Molecule Stabilizers: the Y220X Paradigm. *ACS Chem. Biol.* **2020**, *15*, 657-668, DOI: 10.1021/acschembio.9b00748.

[25] Morris, G. M.; Goodsell, D. S.; Halliday, R. S.; Huey, R.; Hart, W. E.; Belew, R. K.; Olson, A. J., Automated docking using a Lamarckian genetic algorithm and an empirical binding free energy function. *J. Comput. Chem.* 1998, **19***,* 1639-1662, DOI: 10.1002/ (SICI) 1096-987X.

[26] Gasteiger, J.; Marsili, M., Iterative partial equalization of orbital electronegativity- A rapid access to atomic charges. *Tetrahedron* **1980**, 36, 3219-3228, DOI: 10.1016/0040-4020 (80)80168-2.

[27] Seeliger, D.; De Groot, B. L., Liganal docking and binding site analysis with PYMOL and Autodock/Vina.

J. Comput. Aided Mol. Des. **2010**, *24*, 417-422, DOI: 10.1007/s10822-010-9352-6.

[28] Van der Spoel, D.; Lindahl, E.; Hess, B.; Groenhof, G.; Mark, A. E.; Berendsen, H. J. C., GROMACS: fast, flexible, and free. *J. Comput. Chem.* **2005**, *26,* 1701-1718, DOI: 10.1002/jcc.20291.

[29] Sousa da Silva, A. W.; Vranken, W. F., ACPYPE-AnteChamber PYthon Parser interface. *BMC Res. Notes* **2012**, *5*, 367-375, DOI: 10.1186/1756-0500-5-367.

[30] Nose, S.; Klein, M. L., Constant pressure molecular dynamics for molecular systems. *Mol. Phys.* **1983**, *50*, 1055-1076, DOI: 10.1080/00268978300102851.

[31] Nose, S., A molecular dynamics method for simulations in the canonical ensemble. *Mol. Phys.* **1984**, *52,* 255-268, DOI: 10.1080/00268978400101201.

[32] Hoover, W. G., Canonical dynamics: Equilibrium phase-space distributions. *Phys. Rev. A* **1985**, *31,* 1695-1697, DOI: 10.1103/PhysRevA.31.1695.

[33] Berendsen, H. J. C.; Postma, J. P. M.; van Gunsteren, W. F.; Nola, A. D.; Haak, J. R., Molecular dynamics with coupling to an external bath. *J. Chem. Phys.* **1984**, *81,* 3684-3690, DOI: 10.1063/1.448118.

[34] Darden, T.; York, D.; Pedersen, L., Particle mesh Ewald: An N·log(N) method for Ewald sums in large systems. *J. Chem. Phys.* **1993**, *98*, 10089-10092, DOI: 10.1063/1.464397.

[35] Essmann, U.; Perera, L.; Berkowitz, M. L.; Darden, T.; Lee, H.; Pedersen, L. G. J., A smooth particle meshes Ewald method. *Chem. Phys.* **1995**, *103,* 8577-8593. DOI: 10.1063/1.470117.